Spring 2013

Dynamic contact analysis of a piezoelectrically driven ultrasonic crawler-actuator

Dwight Santiago Maness

Department:

DYNAMIC CONTACT ANALYSIS OF A PIEZOELECTRICALLY DRIVEN ULTRASONIC CRAWLER-ACTUATOR

by

DWIGHT SANTIAGO MANESS

A THESIS

Presented to the Faculty of the Graduate School of the

MISSOURI UNIVERSITY OF SCIENCE AND TECHNOLOGY

In Partial Fulfillment of the Requirements for the Degree

MASTER OF SCIENCE IN MECHANICAL ENGINEERING

2013

Approved by

Dr. Daniel Stutts, Advisor
Dr. Douglas Bristow
Dr. Daryl Beetner

PUBLICATION THESIS OPTION

This thesis has been prepared in the form of two papers.

Paper 1. Pages 4–20 has been prepared in the style utilized by the Journal of Sound and Vibration and will be submitted for publication in that journal.

Paper 2. Pages 21–39 has been prepared in the style utilized by the Journal of Sound and Vibration and will be submitted for publication in that journal.

ABSTRACT

A standing wave ultrasonic motor (SWUM) is presented in this thesis. The actuator is piezoelectrically powered and operates in the first and second bending modes to move forwards and backwards, respectively. The kinematic stability of the crawler, backed by experimental results is shown in the first paper presented in this thesis. This study demonstrates that in the absence of a preload or kinematic constraints, the crawler shows vertical stability. A full transient analysis using the finite element method is performed characterizing the speed and contact variables is conducted in the second paper. The results show that given enough time the crawler is inherently stable and will reach a steady state velocity.

ACKNOWLEDGMENTS

First and foremost, I would like to thank my parents Mitch and Eva for their support. Their dedication and love through my years in college made writing this thesis possible. My sister Michelle Nixon and closest friends deserve my wholehearted love as well.

To my advisor Dr. Daniel Stutts whose guidance through these few years have made finishing my research possible. To Dr. Douglas Bristow and Dr. Daryl Beetner for being on my graduate committee and provided guidance to me towards the finality of my work.

There are many people behind the scenes who coached me through some difficult problems. Scott Hamilton, who does a fantastic job as System Administrator and mentored me on the ways of running on the Numerically Intensive Cluster. I am grateful to the DRD and ANSYS support representatives who had a personal hand in troubleshooting hundreds of lines of batch code.

I give credit to my fellow colleagues who pushed me in my endeavors along the way. Chunruong Jiang, who expedited many of the programming and instrumentation tasks that would have taken me twice as long. To Headman Sanei and Yezad Anklesaria both of which deserve my gratitude for suffering with me, through the toils of Finite Element Analysis and LaTeX coding.

TABLE OF CONTENTS

Page

LIST OF ILLUSTRATIONS

LIST OF TABLES

1. INTRODUCTION

With the progress of technology comes the development of actuators of every size, shape and application. Motors almost imperceptible to the human eye are in daily use in nano-electronics. It is in these micro-scale devices that simplistic, lightweight, and high resolution actuation are needed. Unlike larger actuators, micro-motors are simpler in design and often require the use of unique materials capable of actuation at micro-scale. The implementation of piezoelectric materials to fulfill this necessity has led to the development of the contemporary linear piezoelectric ultrasonic motor.

A piezoelectric material is one that takes advantage of the converse piezoelectric effect. Simply put, when a constant electrical field is applied to a piezoelectric material, strain is formed in the material; when alternating current is applied it deforms with a proportional frequency, allowing the vibrational properties to be harnessed. Sashida developed one of the earlier standing wave ultrasonic motors in 1982 that operated at 27.8 kHz and had a 60% efficiency [18]. Following Sashida, Kawamura progressed ultrasonic actuator research in the development of his linear ultrasonic motor [11]. Over the next 20 years standing and traveling wave ultrasonic motors would be developed to provide novel solutions to real world problems [20][13][24][15].

This paper describes a self-driving, linear, standing wave ultrasonic actuator (SWUM). This crawler is the simplest of its kind; consisting of only a beam and a single piezoelectric patch to drive it, similar to what is used in patent 4,612,472 [10]. Shown in Figure 2, the stator consists of a steel beam with strategically placed feet and a piezoelectric patch placed topside. As shown by Zhao in 2011 [22], this single piezoelectric patch when electrically excited will maintain a standing wave within

the stator. More specifically, this sinusoidal forcing causes the piezoelectric ceramic to expand and contract longitudinally. This causes strain on the top surface of the stator and the resulting coupled moment causes the stator to vibrate at the excitation frequency.

The vibrating stator does not produce any useful longitudinal movements without the use of strategically placed feet. He et al demonstrates how the placement of feet along key points on a mode shape can result in bulk movement of a stator [9]. The crawler feet are placed so that the X and Y movements are opposite of each other. This causes the cadence of foot contact to be alternating, allowing movement in the direction of the foot in contact and minimizing interference of the opposite foot.

Many SWUMs require the use of multiple modes working in tandem to achieve a desired movement. In 2001 Kim uses the first longitudinal and fourth bending mode in his stator using four stacked piezoelectric actuators [12]. These actuators that require multiple piezoelectric actuators often require multi-phase excitation to maintain the desired mode shape. However, in 2003 Friend developed a single-phase, single piezoelectric stack actuator capable of bidirectional movement [7]. His tuning fork actuator combines bending and shearing modes that follow a quasi-elliptical path at the contact interface. Driving his actuator in the second tuning fork mode reversed the shearing direction of the forks, allowing the actuator to reverse. The crawler described herein is also a single phase bidirectional actuator, operating with a single piezoelectric element.

Though the crawler is simple in build and function, the mechanisms behind it's movement are unexpectedly complicated. Current papers written on the contact mechanics of vibrating actuators fall into two categories. The first being quasi-static analyses in very discrete time frames as exemplified by Hagedorn and Wallaschek [8]. By removing the temporal component of the problem, the steady-state parameters

are more easily determined. The second category of analysis comes when transient behavior becomes a necessity. In full transient analyses, problems become exponentially harder with the degrees of freedom included. Most papers such as those written by Zhao [23] account for a single degree of freedom or at most two as shown by Liu et al [14] in the analysis of pizza tossing. A primary concern in a full transient analysis is avoiding the stochastic regions in the bifurcation plots of an actuator's kinematic behavior [5]. Variables like foot placement, amplitude of forcing, and contact surface can quickly turn periodic behaviors into fully chaotic scenarios.

Lastly, adding to the kinematic difficulties are the additional complexities that come with contact mechanics: deformation of contacting surfaces causes higher contact time (altering foot phase), increased damping, losses, and micromechanical behaviors that may need to be accounted for.

Due to the complexity of the kinematics and dynamics of such vibratory systems, FEA is typically used as Fernandez demonstrates [6]. Moal [17] and Maeno [16] demonstrate further cases of FEM use to predict the speed and torque values of ultrasonic motors. The free-vibration behavior will first be proven, followed by the full transient problem. Comparisons with experimental results are shown in the second half of the Finite Element Analysis paper.

PAPER

I. KINEMATIC STUDY OF A NOVEL SINGLE-PHASE PIEZOELECTRIC ACTUATOR

Dwight S. Maness, Daniel S. Stutts

MAE Department, Missouri University of Science & Technology,

Rolla, MO 65409

ABSTRACT

An analytical model of a single-phase, ultrasonic, piezoelectric crawler incorporating the kinematics of contact between the crawler feet and the supporting substrate was developed. The model, based upon simple Euler-Bernoulli beam theory and linear piezoelectric behavior, allows the determination of the dynamic normal and tangential reaction forces at the front and rear feet. The normal reaction forces predict a "galloping" motion, and the tangential reactions, based upon simplified contact theory, allow the prediction of the crawler's linear speed. Laser Doppler Vibrometer measurements allowed the determination of an appropriate loss parameter, thereby setting the amplitude of vibration, and an experimental apparatus, developed to measure the front and rear contact duration and phase, confirmed the galloping motion predicted by the model, and measured linear crawler speed also agreed well with model predictions.

1. NOMENCLATURE

$U(x)$	spatial component of displacement solution $u_3(x,t)$
$\eta(x)$	modal participation factor in the solution $u_3(x,t)$
β_n	eigenvalue of the nth mode
L	length of beam
ρ	density beam material
γ	system mechanical damping coefficient
$M(x,t)$	resultant electro-mechanical moment
b	width of beam substrate
y	distance from neutral axis
n	mode number
σ_1^k	stress in the x-direction in the k^{th} layer
Y_1^k	Young's Modulus of each layer
e_{31}^k	piezoelectric stress coefficient
E_3^k	transverse electric field
ε_1^k	normal strain in the x-direction in the k^{th} layer
h_b	height of the stator
h_{PZT}	height of PZT layer
$\phi(x,t)$	spatially distributed applied voltage
$H(x)$	Heaviside step in x
ω_n	natural frequency of n^{th} mode
ζ_n	dimensionless modal damping coefficient
r_n	frequency ratio $\frac{\omega}{\omega_n}$
$\boldsymbol{r_i}$	vector relative to the center of mass
$\boldsymbol{R_i}$	global coordinate vector

2. INTRODUCTION

The piezoelectric actuator, described here as a "crawler," may be classified as a linear standing wave ultrasonic motor or SWUM. Although the crawler described here, similar to the one described in patent 4,612,472 [10], is certainly one of the simplest in its class, it is capable of exhibiting a very rich set of kinematic behaviors. Shown in Figure 1, the stator consists of a steel beam with strategically placed feet and a piezoelectric element placed topside. As shown by Zhao in 2011 [22], this single piezoelectric element when electrically excited will maintain a standing wave within the stator at a frequency equal to that of the excitation frequency.

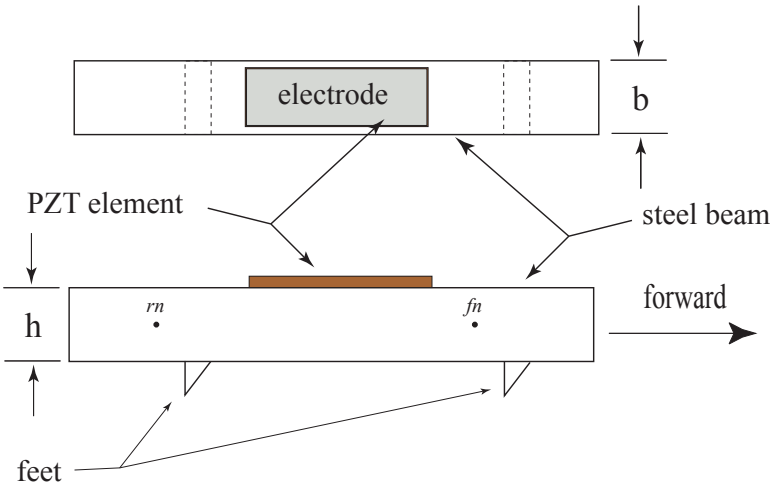

Figure 1. Crawler schematic.

The vibrating stator does not produce any useful longitudinal velocities without the use strategically placed feet. He et al demonstrates how the placement of feet along key points on a vibrating body can result in bulk movement of a stator [9]. The crawler feet are placed so that the front and rear foot movements are opposite of each other. This causes the cadence of foot contact to be alternating, allowing movement in the direction of the foot in contact with minimal drag. The foot dimensions and crawler diagram are found in Table 1 and Figure 2. Three reference frames are used to describe the relevant geometry and kinematics. The upper case vectors ($\boldsymbol{R}$) are

used to describe points on the crawler in the global (X, Y) reference frame, and lowercase ($\boldsymbol{r}$) are used to describe points on the crawler relative to the center of mass at point G in the local (x_G, y_G) reference frame. Static dimensions relative to the local origin at the rear of the crawler on the neutral axis, and located globally by $\boldsymbol{R}_0$, are described using the (x, y) reference frame.

Many SWUMs require the use of multiple modes working in tandem to achieve a desired movement. In 2001, Kim maintains the first longitudinal and fourth bending mode in his stator using four stacked piezoelectric actuators [12]. These actuators that require multiple piezoelectric actuators often require multi-phase excitation to maintain the desired mode shape. However, in 2003 Friend developed a single-phase, single piezoelectric stack actuator capable of bidirectional movement [7]. His tuning fork actuator combines bending and shearing modes that follow a quasi-elliptical path at the contact interface. Driving his actuator in the second tuning fork mode reversed the shearing direction of the forks, allowing the actuator to reverse. The crawler described herein is also a single phase bidirectional actuator, operating with a single piezoelectric element.

Though the crawler is simple in build and function, the mechanisms behind it's movement are complicated. Current papers written on the contact mechanics of vibrating actuators fall into two categories. The first being quasi-static analyses in very discrete time frames as demonstrated by Hagedorn and Wallaschek [8]. By removing the temporal component of the problem, the steady-state parameters are more easily solved. The second category of analysis comes when transient behavior becomes a necessity. In full transient analyses, problems become exponentially harder with the degrees of freedom included. Papers written by Zhao [23] account for a single degree of freedom or at most two as shown by Liu [14] in the analysis of pizza tossing.

Table 1. Material properties and dimensions of crawler

Piezoelectric element	
Material	PZT-5A
Length $(x_2 - x_1)$	1.545 cm
Width	1 cm
Thickness	0.5 cm
Density	7700 kgm^{-3}
Piezoelectric Strain Constant, $d31$	-171×10^{-12} m/V
Stator	
Material	Steel
Young's Modulus	170 GPa
Poisson's Ratio	0.3
Length	2.8 cm
Width	1 cm
Thickness	0.05 cm
Density	7850 kgm^{-3}
x_F (x-coordinate of front foot relative to G)	0.8 cm
x_R (x-coordinate of rear foot relative to G)	2.31 cm
r_{PZT} (neutral axis to the mid-plane of the PZT element)	0.27 cm

A primary concern in a full transient analysis is avoiding the stochastic regions in the bifurcation plots of an actuator's kinematic behavior. Variables like foot placement, amplitude of forcing, and contact surface can quickly turn periodic behaviors into fully chaotic scenarios. Examples of such behavior can be found in the analysis of the bouncing dimer [5] and bouncing rod [21].

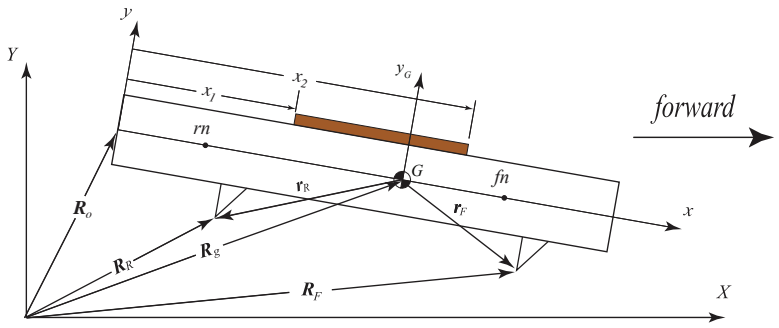

Figure 2. Schematic of relevant crawler kinematic geometry.

Papers similar to those described above by Dorbolo and Liu show stochastic behavior as vibration acceleration exceeds gravity. This paper explores the kinematic behavior and stability of the crawler in the Y-direction, despite flexible body accelerations thousands of times greater then gravity. The behavior in the X-direction is much more complex and will be left for future study. The paper begins with the derivation of the free and forced beam equations before delving into the contact behavior and kinematics of the crawler.

3. ANALYSIS OF FORCED FREE-FREE BEAM

The solution of a Euler-Bernoulli beam, with free-free boundary conditions, as derived by Soedel [19] can be written as:

$$u\left(x,t\right)=U\left(x\right)T\left(t\right) \tag{1}$$

where U(x) represents the spatial solution of the problem represented by

$$U\left(x\right)=\sinh\left(\beta_{n}x\right)+\sin\left(\beta_{n}x\right)+C\left(\cosh\left(\beta_{n}x\right)+\cos\left(\beta_{n}x\right)\right) \tag{2}$$

with,

$$C=-\frac{\sinh\left(\beta_{n}L\right)-\sin\left(\beta_{n}L\right)}{\cosh\left(\beta_{n}L\right)-\cos\left(\beta_{n}L\right)} \tag{3}$$

Passing an alternating current through the piezoelectric (PZT) crystal causes a proportional extension and contraction. The resulting tensile and compressive states on the PZT causes a moment couple about the opposite ends of the PZT element. When bonded to a beam, this moment causes a bending motion. For this derivation extensional effects in the x-direction are ignored; the stator is in pure bending.

The equation of motion for the case described is written as:

$$\rho\,\ddot{u} + \gamma\,\dot{u} + M'' = 0 \tag{4}$$

where M is the mechanical moment, which can be expressed in terms of stress:

$$M(x,t) = b\sum_{k=1}^{2}\int_{y_k}^{y_{k+1}} y\sigma_1^k\; dy \tag{5}$$

and σ_1^k can be represented by

$$\sigma_1^k = Y_k\varepsilon_1^k - e_{31}^k E_3^k \tag{6}$$

where

$$\varepsilon_1^k = yu'' \tag{7}$$

combining (5), (6), and (7) and integrating yields

$$M(x,t) = \sum_{k=1}^{2}\frac{1}{3}\,bY_1^k\left(y_{k+1}^3 - y_k^3\right) - \frac{1}{2}\,be_{31}^k E_3^k\left(y_{k+1}^2 - y_k^2\right) \tag{8}$$

M(x,t) can be rewritten as

$$M(x,t) = \frac{bh^3}{12}Y_1u'' - b\;r_{PZT}\;d_{31}Y_{PZT}\phi(x,t) \tag{9}$$

$$\phi(x,t) = \phi_o\left(H(x-x_1) - H(x-x_2)\right)\sin\omega t \tag{10}$$

ϕ is the the spatially distributed voltage of the PZT starting at x_1 ending at x_2. ϕ_o is the amplitude of the applied voltage. Substitution of (9) and (10) into (4) yields:

$$\rho\ddot{u} + \gamma\dot{u} + YIu^{(4)} = b\;r_{PZT}\;d_{31}Y_{PZT}\phi_o\left(H(x-x_1) - H(x-x_2)\right)\sin\omega t \tag{11}$$

The modal expansion solution to Equation (11) may be written

$$u(x,t) = \sum_{n=1}^{\infty} U_n(x)\eta_n(t) \tag{12}$$

Substitution of (12) into (11) yields:

$$\sum_{n=1}^{\infty} \left(\ddot{\eta}_n + 2\zeta_n\omega_n\dot{\eta}_n + \omega_n^2\eta_n\right) U_n(x) = F_o\left(H(x-x_1) - H(x-x_2)\right)\sin\omega t \tag{13}$$

where

$$F_o = \frac{b\ r_{PZT}\ d_{31}Y_{PZT}\phi_o}{\rho} \tag{14}$$

$$\omega_n = \beta_n^2\frac{YI}{\rho} = \frac{(\beta_n L_b)^2}{L_b^2}\sqrt{\frac{YI}{\rho}} \tag{15}$$

and

$$2\zeta\omega_n = \frac{\gamma}{\rho} \tag{16}$$

Multiplying by $U_m(x)$ and integrating over the domain yields:

$$\begin{aligned} &\sum_{n=1}^{\infty} \left(\ddot{\eta}_n + 2\zeta_n\omega_n\dot{\eta}_n + \omega_n^2\eta_n\right) \int_0^{L_b} U_n(x)U_m(x)\ dx \\ = \quad & F_o\int_0^{L_b} \left(H(x-x_1) - H(x-x_2)\right) U_m(x)\sin\omega t\ dx \end{aligned} \tag{17}$$

The result, by orthogonality, for $m = n$, is given by

$$\ddot{\eta}_n + 2\zeta_n\omega_n\dot{\eta}_n + \omega_n^2\eta_n = F_n(t) \tag{18}$$

where:

$$F_n(t) = \frac{br_{PZT}Y_{PZT}\phi_o\left(U_n'(x_2) - U_n'(x_1)\right)}{\rho N_n}\sin\omega t \tag{19}$$

$$N_n = \int_0^{L_b} U_n^2(x)\ dx \tag{20}$$

$$\eta_n(t) = \Lambda_n \sin(\omega_n \sqrt{1-\zeta_n^2} t - \phi_n) \tag{21}$$

$$\Lambda_n = \frac{\Gamma_n}{\omega_n \sqrt{(1-r_n^2)^2 + (2\zeta_n \omega_n r_n)^2}} \tag{22}$$

$$\Gamma_n = \frac{b r_{PZT} Y_{PZT} \phi_o \left(U_n'(x_2) - U_n'(x_1)\right)}{\rho N_n} \tag{23}$$

and

$$\phi_n = \begin{cases} \arctan\left(\frac{2\zeta_n\omega_n}{1-r_n^2}\right), & \text{if } r_n \leq 1 \\ \pi + \arctan\left(\frac{2\zeta_n\omega_n}{1-r_n^2}\right), & \text{for } r_n > 1 \end{cases} \tag{24}$$

4. ANALYSIS OF BOUNCING BEHAVIOR

In this paper the assumption is made that the rotation of the center of gravity (θ_G) is negligible and the contacting interfaces are assumed to be rigid. The subscript i will be used to indicate a foot located at location x_i for any number of feet located between 0 to L:

$$Y(x_i, t) = Y_i(t) \tag{1}$$

$$r_i = (x_i - x_G) \tag{2}$$

$$\ddot{u}(x_i, t) = \ddot{u}_i(t) \tag{3}$$

Defining the equations of motion:

$$m\ddot{Y}_G(t) = \sum_i N_i - mg \tag{4}$$

$$I_g \ddot{\theta}_G = \sum_i r_i \times N_i \tag{5}$$

A function Y(x,t) is created to represent a global coordinate dimension to any point on the neutral axis of the actuator.

$$Y(x,t) = u(x,t) + (x - x_G)\theta(x,t) + Y_G(t) + Y_0 \tag{6}$$

where $Y_G(t)$ is a global coordinate dimension representing the distance from the ground to the unrotated rigid body frame, and Y_0 is the initial height of the center of gravity at time equals zero. $\theta(x,t)$ and $Y_G(t)$ are the rigid body components of movement, meaning they are invariant with respect to x. The second derivative of Equation (6) is taken and integrated with respect to density terms to obtain an equation for inertia.

$$\rho bh \int_0^L \ddot{Y}(x,t)\,\mathrm{d}x = \rho bh \int_0^L \ddot{u}(x,t)\,\mathrm{d}x + (\frac{x^2}{2} - x(x_G))\ddot{\theta}(t) + \rho bhL\ddot{Y}_G(t) \tag{7}$$

A beam vibrating in the symmetric first mode has the integral $\int_0^L \ddot{u}(x,t)\,\mathrm{d}x$ approximately equal to 0. Additionally, a crawler with feet of negligible mass placed nearly symmetric about the center of gravity has the second term in (7) also equal to zero. In other words, treating x_G like a variable:

$$\lim_{x_G \to L/2} \left[\frac{x_2}{2} - x(x_G)\right]_0^L = 0 \tag{8}$$

therefore, Equation (7) is reduced to a simpler form.

$$\rho bh \int_0^L \ddot{Y}(x,t)\,\mathrm{d}x = \rho bhL\ddot{Y}_G(t) \tag{9}$$

The remainder of this paper will delve into the three possible cases of contact for the crawler: single foot contact, multi-foot contact, and no contact. For any foot in

contact at location x_i,

$$Y_i(t) = 0 = Y_G(t) + (x_i - x_G)\theta(t) + u_i(t) + Y_0 \tag{10}$$

solving for $Y_G(t)$ and using Equations (4) and (9) yields the normal force for the foot in question.

$$N_i = \frac{I_G m \left(g - \ddot{u}_i(t)\right)}{I_G + m \left(x - x_G\right)^2} \tag{11}$$

From this equation the rigid body rotation and global coordinate to the center of gravity can easily be solved for.

$$\theta(t) = \frac{m(x_i - x_G)^2}{I_G + m(x - x_G)^2} \left(\frac{gt^2}{2} - u_i(t) + \dot{u}_i(t_0)t + u_i(t_0) \right) + \dot{\theta}(t_0)t - \theta(t_0) \tag{12}$$

$$Y_G(t) = u(x_G, t) + (\Gamma - 1)u_i(t) - \frac{\Gamma g t^2}{2} - \Gamma \upsilon(t) - s(t) + Y_0 \tag{13}$$

where,

$$\Gamma = \frac{m(x_i - x_G)^2}{I_G + m(x_i - x_G)^2} \tag{14}$$

$$\upsilon(t) = \dot{u}(t_0)t + u_i(t_0) \tag{15}$$

$$s(t) = (x_i - x_G) \left(\dot{\theta}(t_0)t - \theta(t_0) \right) \tag{16}$$

A similar process is followed for solving the case of multiple foot contact. The problem will be solved assuming that only two feet are present at locations x_i and x_j and are in contact at the same time, thus

$$Y_i(t) = Y_j(t) = 0. \tag{17}$$

Following a similar process to single foot contact the kinematics and forces on the crawler can be achieved.

$$\theta(t) = \frac{u_j(t) - u_i(t)}{x_i - x_j} \tag{18}$$

$$N_i = \frac{(x_G - x_j)\left(x_i(\ddot{u}_j + g) - x_j(\ddot{u}_i + g) + x_G(\ddot{u}_i - \ddot{u}_j)\right) - I_G(\ddot{u}_i - \ddot{u}_j)}{(x_i - x_j)^2} \tag{19}$$

$$N_j = \frac{(x_i - x_G)\left(x_i(\ddot{u}_j + g) - x_j(\ddot{u}_i + g) + x_G(\ddot{u}_i - \ddot{u}_j)\right) + I_G(\ddot{u}_i - \ddot{u}_j)}{(x_i - x_j)^2} \tag{20}$$

$$Y_G(t) = u_G(t) + \left(\frac{u_i(t)(x_G - x_j) + u_j(t)(x_i - x_G)}{x_i - x_j}\right) + Y_0 \tag{21}$$

The last case is one of no foot contact, specifically:

$$N_i = N_j = 0 \tag{22}$$

Following this, the equations of motion become synonymous with parabolic motion equations.

$$Y_G(t) = Y_0 + Y_G(t_0) + \dot{Y}_G(t - t_0) - \frac{g}{2}(t - t_0)^2 \tag{23}$$

where θ, having no forces to drive it simply becomes a product of it's previous state

$$\theta(t) = \dot{\theta}(t_0)t + \theta(t_0) \tag{24}$$

In order to solve for t_n, the time of contact for the nth collision, Equation (23) is set equal to the expression of $Y_G(t)$ of when the foot is to be in contact next.

$$Y_G(t_0) + \dot{Y}_G(t_n - t_0) - \frac{g}{2}(t_n - t_0)^2 = -\left(\omega(t_n) + u_i(t_n) + Y_0\right) \tag{25}$$

5. RESULTS

A 30 V signal is applied to the piezoelectric element with the first natural frequency of 32.3 kHz found via Equation (15). A material damping parameter of ζ=0.001 is used to get the amplitude shown in Figure 4a. When compared to the experimental result, found by using a scanning laser doppler vibrometer (LDV) to the underside of the crawler, the amplitude is shown to be in agreement as shown in Figure 4c. Additionally, the damping parameters are in agreement with the maple simulation using ζ=0.001 and the finite element method using ζ=0.0012.

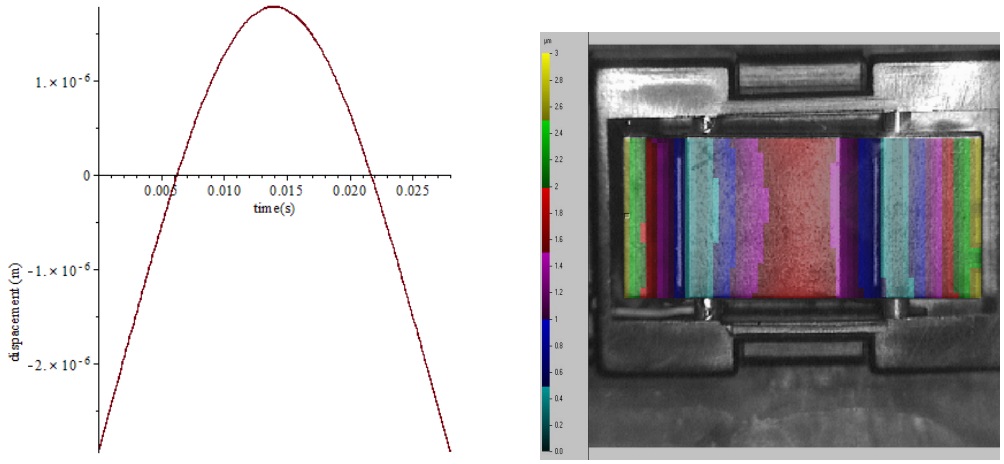

(a) Maximum deflection of the first mode using Maple.

(b) Experimental LDV scan of underside of crawler showing deflection.

Figure 3. Comparison of maximum deflection of crawler found via simulation and experimentation.

The forced vibration behavior is superimposed onto a rigid contacting interface and the vertical stability is observed. A vertical loss parameter is added via a coefficient of restitution that is varied to 0.3, 0.6, and 0.9. The crawler is released from an initial height of 13.75 μm and allowed to contact and bounce off of the rigid surface. The transient vibrational effects of the crawler as well as the vibrations transmitted through contact are ignored. Rotation about the center of gravity is assumed to be small and the crawler operates on a frictionless surface; the goal of

this simulation is to prove vertical periodicity and stability of the crawler. As shown in Figure 4, despite the initial conditions the crawler always reaches an equilibrium height of 2.75 mm, with minimal bounce. The explanation for this remarkable behavior can be found in examining the nature of the combined rotor-stator design the crawler consists of.

An ultrasonic actuator typically consists of a stator being moved by a powered rotor with a preload, guaranteeing contact and predictable shear friction behavior. The crawler, having the stator itself powered and acting as the rotor, does not have this preload allowing free rigid body and flexure of the center of gravity. This rigid body effect is found in Figure 4 which shows the foot is in contact with the ground near it's maximum amplitude. It would seem intuitive that at the point of contact, the acceleration of the crawler foot (which exceeds gravity by a factor of 2500) would immediately launch the crawler into the air. On the contrary, a specific chain of events must occur before the foot can propel the crawler upwards.

Due to the large differences between acceleration and gravity of the foot, a generic sine and cosine wave is shown in Figure 5 to illustrate this concept. Three events must happen simultaneously in order for the crawler to propel itself upwards: the foot must be in contact with the ground, the foot velocity must be directed downwards, and the acceleration of the foot must exceed gravity. When the foot fulfills all of these conditions, it "transmits" energy as indicated by region one in Figure 5. In this state of transmission the foot rebounds, causing an upward acceleration of the center of gravity. Adversely, when the foot velocity and acceleration are directed upwards the crawler reaches a state of absorption. It is in this absorbing domain shown in region two, where there is a net energy loss and the crawler sticks to the surface. Similar behavior occurs in the other two regions but are areas of improbable contact. Improbable since fulfilling these scenarios will either require a preload or eccentric rotation about the center of gravity to maintain contact. Since there is no

preload and rotation is assumed to be negligible, these scenarios are not considered. The results of the crawler show that each foot lands on the edge of the transmitting region. This is due to the crawler being able to reach an equilibrium rigid body height near the maximum amplitude of the feet, where the foot velocity is near zero. Coincidentally, this is the reason why the lack of preload does not allow the crawler enough rebounding to become airborne, ensuring periodic steady state behavior given enough time.

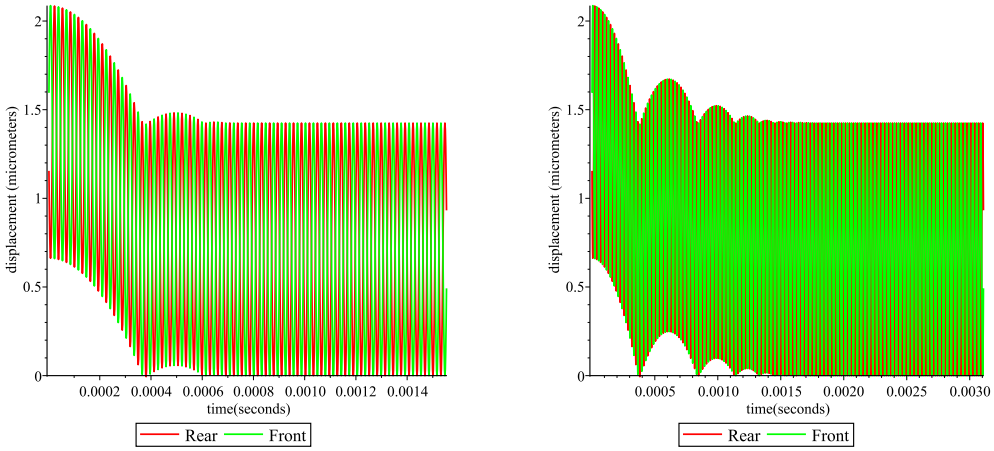

(a) ϵ=0.3

(b) ϵ=0.6

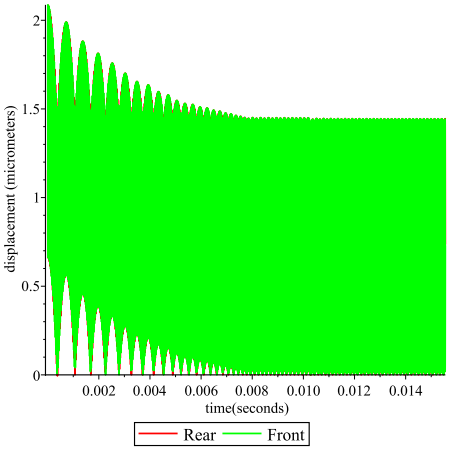

(c) ϵ=0.9

Figure 4. Steady state behavior of crawler at various coefficients of restitution.

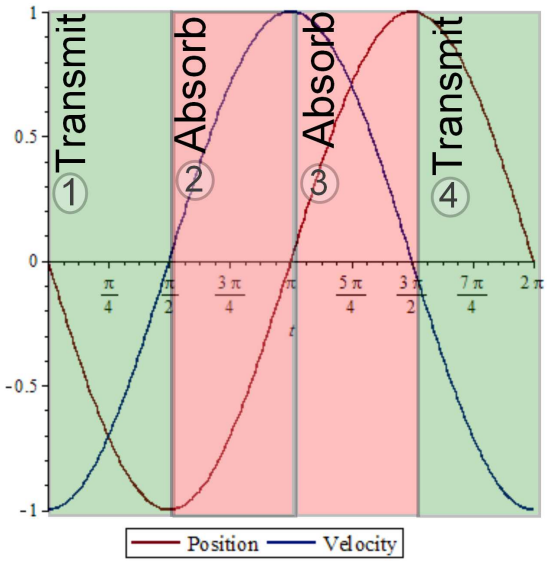

Figure 5. Illustration of foot phase and resulting kinematic energy

6. CONCLUSION

The crawler SWUM has shown that an actuator of simple design can demonstrate complex behaviors. This paper takes the unique approach of analyzing the kinematics of a bouncing and vibrating body, which from the outcome of this study demonstrates that there are differences with similar studies of bouncing bodies. Papers involving preloads or rigid objects rebounding on bouncing platforms show instabilities at accelerations much higher then gravity. Most analyses of this type stay far below the acceleration of gravity region to avoid such stochastic behaviors.

The stability of this crawler is shown and is proven that given a wide array of damping parameters and initial heights, the crawler inevitably reaches a state of periodicity. Some bouncing is expected initially with primary driving variables being the initial kinematic state, excitation amplitude, and foot cadence. Landing at the boundary of the absorb/transmit region means that little energy is transmitted through the stator-rotor with the net outcome being a decay of the bouncing. This is shown to be the case for the crawler contacting multiple surfaces.

In the process of creating the mathematical model described herein, the full X and Y behaviors were sought, specifically the steady state velocity of the X-direction. To accurately produce this, the rotational behavior about the center of gravity and deformation would have to be included. As previously stated many authors opt to solve either the reduced degree of freedom problem (as shown in this paper) or a quasi-static (hertzian type) model to avoid transient behavior. If both rotation and deformation were included, the problem bypasses these simplifications and becomes exponentially more difficult to solve for. This opens up the possibility of future study to develop such a deformable, three degree of freedom, transient model.

II. FINITE ELEMENT ANALYSIS OF SINGLE-PHASE, BI-DIRECTIONAL, ULTRASONIC CRAWLER-ACTUATOR

Dwight S. Maness, Daniel S. Stutts

MAE Department, Missouri University of Science & Technology,

Rolla, MO 65409

ABSTRACT

The dynamics of a standing wave linear type actuator crawler is modeled using the finite element method. A transient multi-body, nonlinear contact model is developed to predict the contact behavior between the vibrating body and target surface. Crawler behaviors are confirmed through experimental means. Comparisons of finite element and experimentation in steady-state yield similar results.

7. NOMENCLATURE

T	Period of Vibration
$[M]$	Mass Matrix
$[K]$	Stiffness Matrix
$[C]$	Structural Damping Matrix
u_n	Nodal Displacement Vector at Time t_n
$[F]$	Forcing Function Matrix
$[T]$	Stress Vector
$[D]$	Electric Flux Density Vector
$[c^E]$	Elasticity Matrix
$[\epsilon]^S$	Dielectric Matrix
$[S]$	Elastic Strain Vector
$[E]$	Electric Field Intensity Vector
$[K]^Z$	Piezoelectric Coupling Matrix
$[K]^D$	Element Dielectric Permitivity Coefficient
$[L]$	Vector of Nodal, Surface, and Body Charges

8. INTRODUCTION

This paper describes a self-driving, linear, standing wave ultrasonic actuator (SWUM). This crawler is the simplest of its kind; consisting of only a beam and a single piezoelectric patch to drive it, similar to what is used in patent 4,612,472 [10]. Shown in Figure 1, the stator consists of a steel beam with strategically placed feet and a piezoelectric patch placed topside. As shown by Zhao in 2011 [22], this single piezoelectric patch when electrically excited will maintain a standing wave within the stator. More specifically, this sinusoidal forcing causes the piezoelectric ceramic to expand and contract longitudinally. This causes strain on the top surface of the

stator and the resulting coupled moment causes the stator to vibrate at the excitation frequency.

The vibrating stator does not produce any useful longitudinal movements without the use of strategically placed feet. He et al demonstrates how the placement of feet along key points on a mode shape can result in bulk movement of a stator [9]. The crawler feet are placed so that the X and Y movements are opposite of each other. This causes the cadence of foot contact to be alternating, allowing movement in the direction of the foot in contact and minimizing interference of the opposite foot. The foot dimensions and general crawler dimensions are found in Table 1.

Many SWUMs require the use of multiple modes working in tandem to achieve a desired movement. In 2001 Kim uses the first longitudinal and fourth bending mode in his stator using four stacked piezoelectric actuators [12]. These actuators that require multiple piezoelectric actuators often require multi-phase excitation to maintain the desired mode shape. However, in 2003 Friend developed a single-phase, single piezoelectric stack actuator capable of bidirectional movement [7]. His tuning fork actuator combines bending and shearing modes that follow a quasi-elliptical path at the contact interface. Driving his actuator in the second tuning fork mode reversed the shearing direction of the forks, allowing the actuator to reverse. The crawler described herein is also a single phase bidirectional actuator, operating with a single piezoelectric element.

Table 1. Crawler Properties

Piezoelectric Patch	
Material	PZT-5A
Length	2.8 cm
Width	1 cm
Thickness	0.5 cm
Density	7700 kgm^{-3}
Piezoelectric Strain Constant, $d31$	-171×10^{-12} m/V
Stator	
Material	Steel
Young's Modulus	170 GPa
Poisson's Ratio	0.3
Length	1.545 cm
Width	1 cm
Thickness	.05 cm
Density	7850 kgm^{-3}
x_F	0.8 cm
x_R	2.31 cm

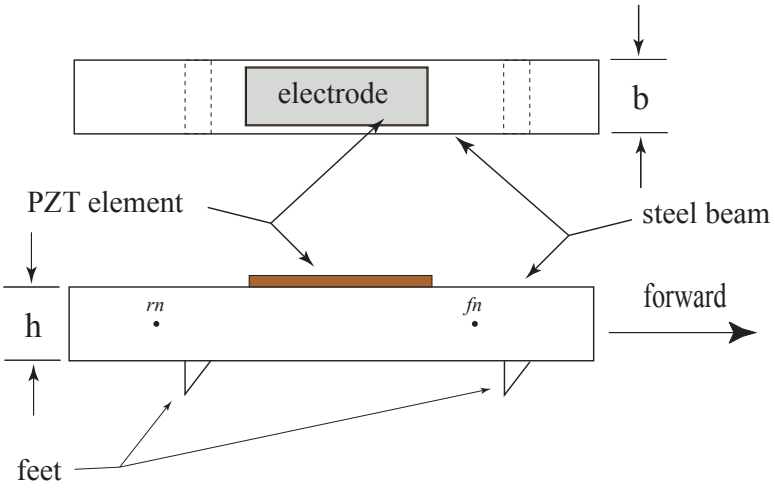

Figure 1. Crawler schematic.

Though the crawler is simple in build and function, the mechanisms behind it's movement are unexpectedly complicated. Current papers written on the contact mechanics of vibrating actuators fall into two categories. The first being quasi-static analyses in very discrete time frames as exemplified by Hagedorn and Wallaschek [8].

By removing the temporal component of the problem, the steady-state parameters are more easily determined. The second category of analysis comes when transient behavior becomes a necessity. In full transient analyses, problems become exponentially harder with the degrees of freedom included. Most papers such as those written by Zhao [23] account for a single degree of freedom or at most two as shown by Liu et al [14] in the analysis of pizza tossing. A primary concern in a full transient analysis is avoiding the stochastic regions in the bifurcation plots of an actuator's kinematic behavior [5]. Variables like foot placement, amplitude of forcing, and contact surface can quickly turn periodic behaviors into fully chaotic scenarios. Lastly, adding to the kinematic difficulties are the additional complexities that come with contact mechanics: deformation of contacting surfaces causes higher contact time (altering foot phase), increased damping, losses, and micromechanical behaviors that may need to be accounted for.

Due to the complexity of the kinematics and dynamics of such vibratory systems, Finite Element Analysis (FEA) is typically used as Fernandez demonstrates [6]. Moal [17] and Maeno [16] demonstrate further cases of FEA use to predict the speed and torque values of ultrasonic motors. The free-vibration behavior will first be proven, followed by the full transient problem. Comparisons with experimental results are shown in the second half of the paper.

9. FREE VIBRATION

9.1. FINITE ELEMENT ANALYSIS. The crawler model was developed using ANSYS 14 and the adaptive parametric design language (APDL) functionality. The piezoelectric patch is lined with multiphysics elements while the stator is lined with flexible structural elements that propagate the piezoelectric excitation into the

proper deformations and outputs. Both the piezoelectric and stator elements use constant plane stress assumptions.

Modal analysis determines the natural frequencies of the unpowered crawler. The natural frequencies forthe first seven predominant bending modes are given in Table 2.

Table 2. Natural Frequencies in free-vibration given in FEA.

Mode	Natural Frequency (KHz)
1	29.11
2	67.56
3	85.68
4	110.68
5	154.99
6	170.97
7	192.54

A harmonic analysis is performed to display the amplitude and mode shape of the crawler in steady state at a particular frequency. The harmonic analysis of the crawler is forced at each resonant frequency with the damping ratio $\zeta = 0.12\%$. Inspection of the foot cadence and direction for the first and third mode show the greatest likelihood of bidirectional behavior. The results of the simulation can be seen in Figure 2. The color spectrum displayed in the figure show the spectrum of Y-direction displacements with respect to the undeformed model.

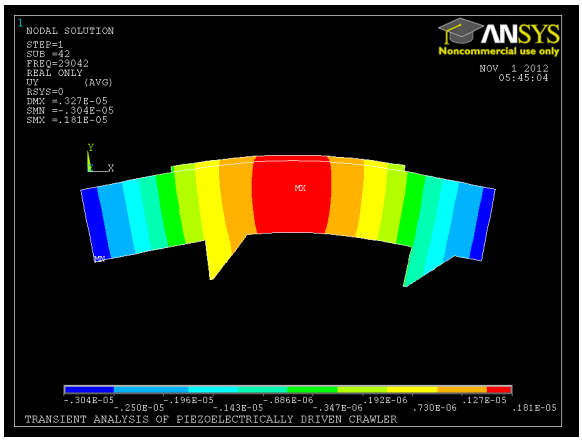

(a) First Mode

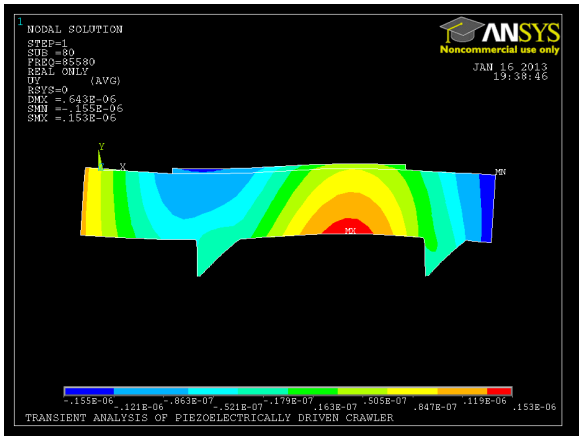

(b) Third Mode

Figure 2. Mode shape of the first and third modes using a damping ratio of $\zeta = .12\%$.

9.2. EXPERIMENTAL RESULTS. An HP 4294A impedance analyzer is used to provide verification of the natural frequencies and damping ratios. An impedance trace shows that the forward and reverse modes lie at 30.71 and 89.36 KHz, respectfully. The same impedance analyzer can output the piezoelectric equivalent circuit for our crawler. Using the equivalent circuit model, the parameters are: $R_1 = 312.17\ \Omega$, $L_1 = 667.49$ mH, $C_1 = 40.30$ pF, $C_0 = 3.51$ nF for the forwards mode and $R_1 = 136.83\ \Omega$, $L_1 = 261.27$ mH, $C_1 = 12.12$ pF, $C_0 = 3.51$ nF for the reverse

mode. The use of Equation (1) gives a damping ratio of approximately $\zeta = 0.0012$ and $\zeta = 0.000466$ for the forward and reverse modes, respectively.

$$\zeta = \frac{R_1}{2}\sqrt{\frac{C_1}{L_1}} \tag{1}$$

A scanning laser doppler vibrometer shows the maximum amplitudes of the crawler at every point in it's length. Comparing the magnitudes of this figure with that shown for the finite element (Figure 2a) shows agreeable causatum: amplitudes at the feet are at 0.3-0.6 micrometers, maximum displacements at the end are approximately 3 micrometers, and displacement at the center of the beam is 0.16-0.18 micrometers. A scan of the reverse mode is not obtained for this paper.

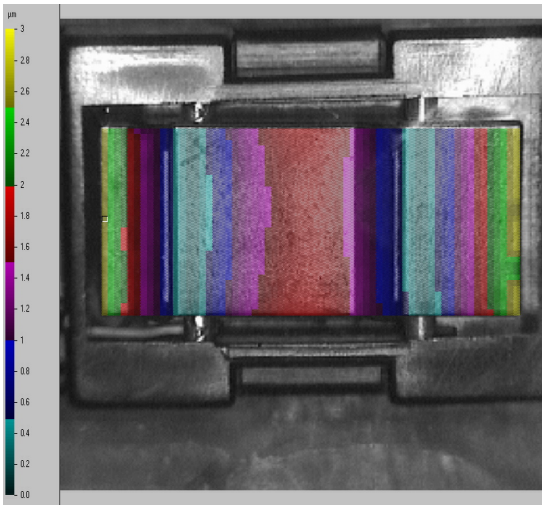

Figure 3. Displacement scan of LDV for crawler SWUM.

10. FORCED VIBRATION AND TRANSIENT CONTACT

10.1. FINITE ELEMENT ANALYSIS. To solve the difficulties of this problem, the harmonic behavior is juxtaposed onto a contacting surface. Thus, the nonhomogeneous forced vibration equation becomes coupled with a nonlinear transient contact problem. Relevant assumptions and methods from the ANSYS APDL

Theory Reference [2] are summarized below to illustrate the amalgamation of equations involved in solving this model. Shown in Equation (1) is a general equation for a second order forced system.

$$[M]\ddot{u} + [C]\dot{u} + [K]u = F \tag{1}$$

The Newmark time integration method is used for an implicit expression of Equation (1) to solve for the dependent variable in question, u. Following that method, the dependent variables and derivatives of the previous state at time t_n are known:

$$\begin{aligned}&\left(a_0[M] + a_1[C] + [K]\right) u_{n+1} \\ &= F + [M]\left(a_0 u_n + a_2\dot{u}_n + a_3\ddot{u}_n\right) + [C]\left(a_1 u_n + a_4\dot{u}_n + a_5\ddot{u}_n\right)\end{aligned} \tag{2}$$

$$\dot{u}_{n+1} = \dot{u}_n + a_6\ddot{u}_n + a_7\ddot{u}_{n+1} \tag{3}$$

$$\ddot{u}_{n+1} = a_0\left(u_{n+1} - u_n\right) - a_2\dot{u}_n - a_3\ddot{u}_n \tag{4}$$

where $a_0 ... a_7$ are Newmark time integration coefficients [4]. Additionally, since the multi-physics model incorporates piezoelectric actuation, Equation (1) will need to be augmented with the governing equations for piezoelectric materials.

$$\begin{bmatrix} T \\ D \end{bmatrix} = \begin{bmatrix} [c^E] & [e] \\ [e]^T & -[\epsilon]^S \end{bmatrix} \begin{bmatrix} S \\ -E \end{bmatrix} \tag{5}$$

Through the application of variational principle and finite element discretization shown in [1], the final coupled transient piezoelectric matrices are produced.

$$\begin{bmatrix} [M] & [0] \\ [0] & [0] \end{bmatrix} \begin{bmatrix} \ddot{u} \\ \ddot{V} \end{bmatrix} + \begin{bmatrix} [C] & [0] \\ [0] & [0] \end{bmatrix} \begin{bmatrix} \dot{u} \\ \dot{V} \end{bmatrix} + \begin{bmatrix} [K] & [K^Z] \\ [K^Z]^T & [K^D] \end{bmatrix} \begin{bmatrix} u \\ V \end{bmatrix} = \begin{bmatrix} F \\ L \end{bmatrix} \tag{6}$$

Lastly, the contact method used to derive interaction with a surface is a simple Coulomb friction model using the augmented Lagrangian method. This method is used to update the contact pressure at every iteration so that the contact pressure represented by:

$$P = \begin{cases} 0, & \text{if } u_n > 0 \\ K_n u_n + \lambda_{i+1}, & \text{if } u_n \leq 0 \end{cases} \tag{7}$$

$$\lambda_{i+1} = \begin{cases} \lambda_i + K_n u_n, & \text{if } u_n > \epsilon \\ \lambda_i, & \text{if } u_n \leq \epsilon \end{cases} \tag{8}$$

where K_n and u_n are the normal contact stiffness and gap size, respectively; λ is the lagrange multiplier component at iteration i, while ϵ is the contact tolerance.

In addition to the elements already in place, contact elements are placed so the desirable contact parameters can be outputted. A rigid line is used as the contacting interface to reduce simulation time and resources, that would otherwise be necessary for a fully deformable surface. Additionally, the simulation is more numerically stable in element formulations between time steps with only one deformable surface. The contact elements were superimposed over the structural elements that made up the feet. Similarly, rigid target elements were placed over the rigid line intended to act as the surface interface.

In this transient solution, sinusoidal forcing with an amplitude of 30 V is used. 80,000 substeps over the course of 0.13 seconds are specified amounting to

approximately 20 substeps/cycle to minimize aliasing. Three surfaces are used in this simulation: Delrin, Nylon, and Plexiglas. The coefficients of kinetic friction were found experimentally, using the method shown in the experimental results. Figure 6 shows how a typical output for an finite element simulation would look; shown is the output for $\mu = 0.25$.

Sought after is the behaviour of the crawler as it reaches steady-state conditions. In Figure 4a and 4b are shown contact and shear friction pressures that look anything but steady-state. The normal pressure at times deviates at 15 MPa, while the shear friction show seemingly unpredictable negative and positive behavior. However, the contrary is shown in results for the contact status and velocity. Shown in Figure 4c is the state of the crawler contact at any moment in time. A value of 1 correlates to the crawler in near contact, values above that show the actuator in full slip contact conditions. Viewing the full record for contact status, the contact is shown to be periodic in contact duration for the majority of the record.

Figure 8 presents the transient behavior of the crawler as it reaches steady-state. The large sinusoidal fluctuation is from the inclusion of both the rigid body and extensional mode velocities. A listing of the averaged steady-state results are shown in Table 3, to give a valid comparison between the surfaces. The duty cycle shown in this figure uses Equation (9) and data from the contact status to determine an average steady-state contact duty cycle.

$$Duty\ Cycle = \frac{t_{contact}}{T} \times 100\% \tag{9}$$

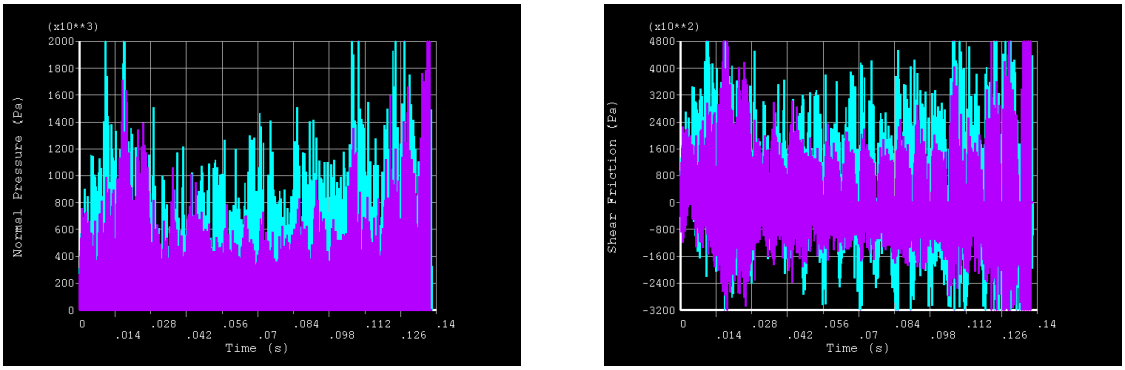

(a) Contact Pressure

(b) Shear Friction

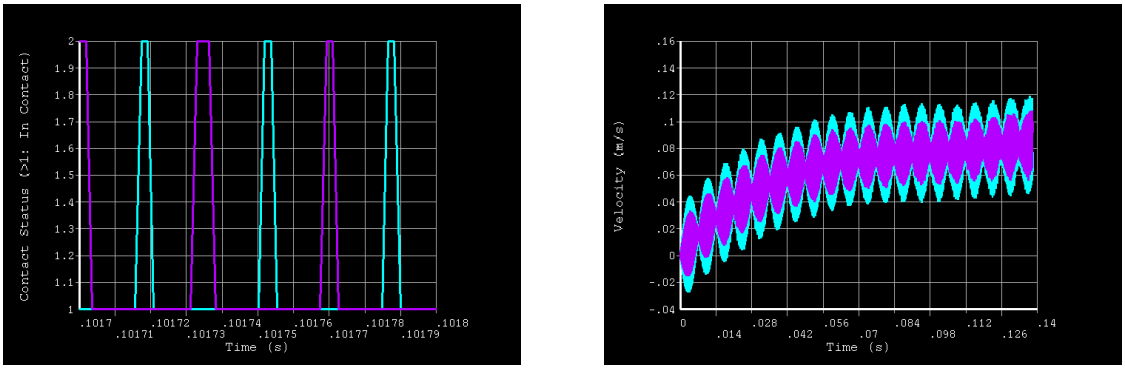

(c) Contact Status

(d) X-direction Velocity

Figure 4. Sample output of dynamic forces and kinematic parameters for crawler running on Delrin ($\mu = 0.25$). Front foot represented by blue and rear foot represented by magenta

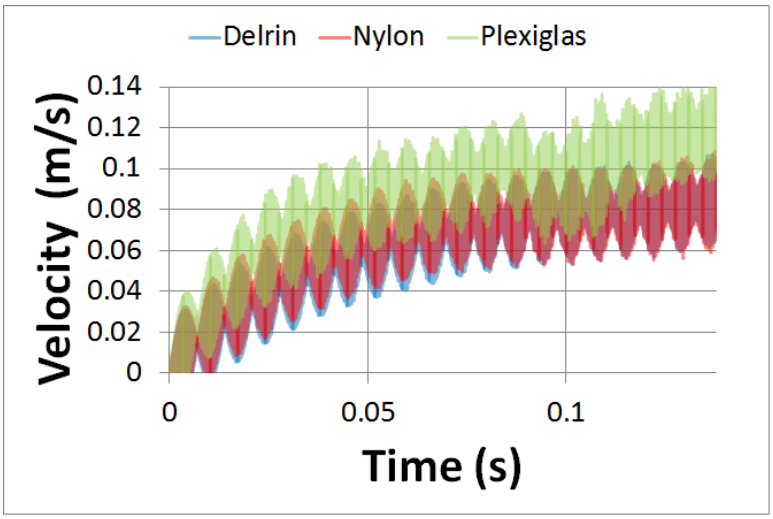

Figure 5. Transient x-direction velocities of the crawler.

Table 3. Summary of Averaged Finite Element Results

Comparison of Contact Duration				
Material	*Dynamic Coefficient of Friction*	*Duty Cycle Front / Rear*	*Contact Force Front / Rear*	*Steady-State Velocity*
Delrin	0.25	15% / 30%	0.8 N / 0.5 N	0.08 m/s
Nylon	0.30	18% / 33%	1.2 N / 0.8 N	0.08 m/s
Plexiglas	0.50	30% / 60%	2.7 N / 1.1 N	0.11 m/s

The same method is performed to analyze motion in the third mode. Due to a significantly lower vibration amplitude in the reverse mode, the data becomes more difficult to examine. Figure 6a is the velocity displayed for the crawler on Delrin, showing that the low rigid body velocity is obscured by the extensional mode velocity. Only upon viewing the displacement and adding a linear interpolation, can a hypothesis for the steady-state velocity be made (Figure 6b). The outcome of this linear interpolation (shown in the figure) is a steady state velocity that approaches 0.7 mm/s. The simulations for Nylon and Plexiglas are identical.

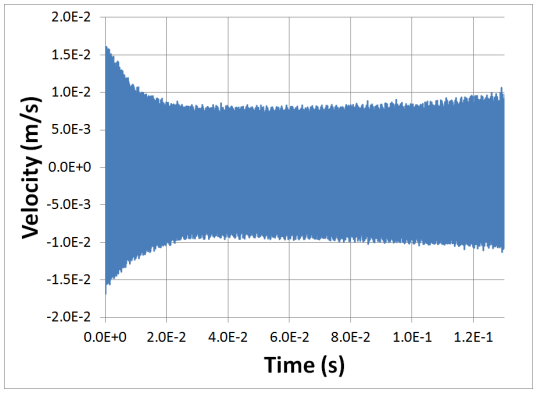

(a) X-direction velocity for crawler in third mode

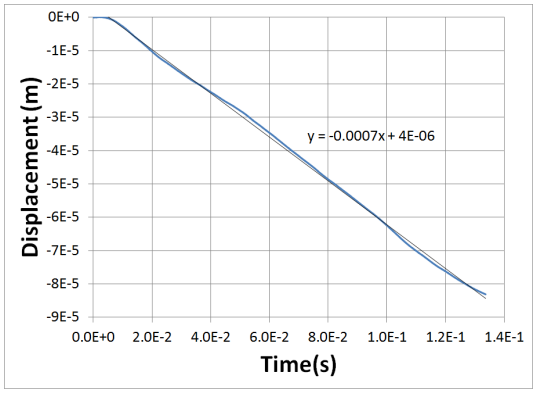

(b) Displacement in third mode exhibiting backwards behavior (linear interpolation included)

Figure 6. Transient data output for crawler in third mode, shown for Delrin

10.2. EXPERIMENTAL RESULTS. Figure 7 shows two simple, custom made devices used to measure the contact friction, velocity, and foot cadence. The device shown in Figure 7a is created to determine the contact duration of the front and rear feet. The objective is to be able to compare the timing and phase of the feet relative to each other, in addition to the crawler as a whole. For this device, two sets of parallel plates are energized with a 5 V source. When the front foot is in contact for the set of front plates, the signal reads low (0 V). Likewise, when the foot is airborne it will read high (5 V). A sampling of the transient behaviour is shown

in Figure 8, while an averaged set of steady state data is shown in Figure 4. The assumption is made that the contact duration on the copper is similar to that of the three materials, absent sticking. Comparisons with Table 3 show this is a reasonable statement.

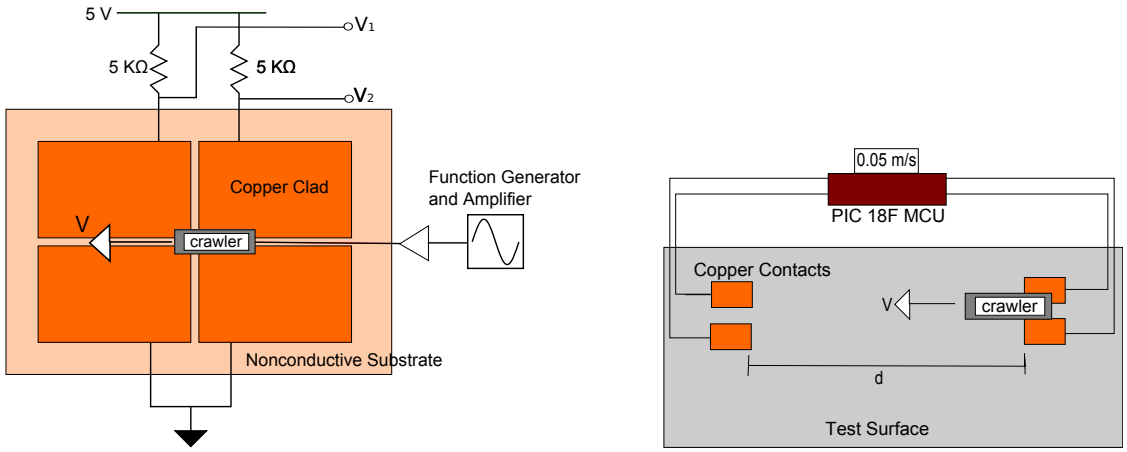

(a) Contact duty cycle device.

(b) Velocity and friction coefficient device.

Figure 7. Copper contact devices for verifying contact behaviours.

The transient behavior in Figure 8 shows that it takes the crawler approximately 2 microseconds to reach steady-state like behaviour. For 0.75 microseconds, the rear foot appears to be dragging on the ground until the excitation reaches an appreciable amplitude. Conversely, the front foot appears to be in the air for more than 2 microseconds before reaching semi-periodic timing. Upon closer observation of the front foot data, high frequency noise is seen during that period around the 5 V mark. This can be attributed to aliasing of our measuring device and is exhibiting some very high frequency bouncing of the front foot prior to reaching the correct sync with the rear. The previously stated 2 microsecond steady-state time is in stark contrast to the finite element results that show steady-state behaviour at approximately 0.1 seconds. This differing steady state behaviour can be attributed to the damping losses that finite element analysis does not account for. Apart from the

structural damping ratio specified, there are no other significant structural or viscous losses accounted for in the finite element model.

Examining the data shown in steady-state (Figure 9), shows that as one foot leaves the ground the other is in contact soon afterwards, i.e. there is a very short time they are both in contact. The conclusion is made that the crawler moves with each foot galloping in succession, similar to how Zhao in 2011 demonstrates his two-phase actuator [22]. Comparing the full length of the experimental data with that found in the finite element model, the high frequency bouncing observation is again seen. Although the crawler moves with steady-forward velocity, the contact behavior seems to be quasi steady-state at best.

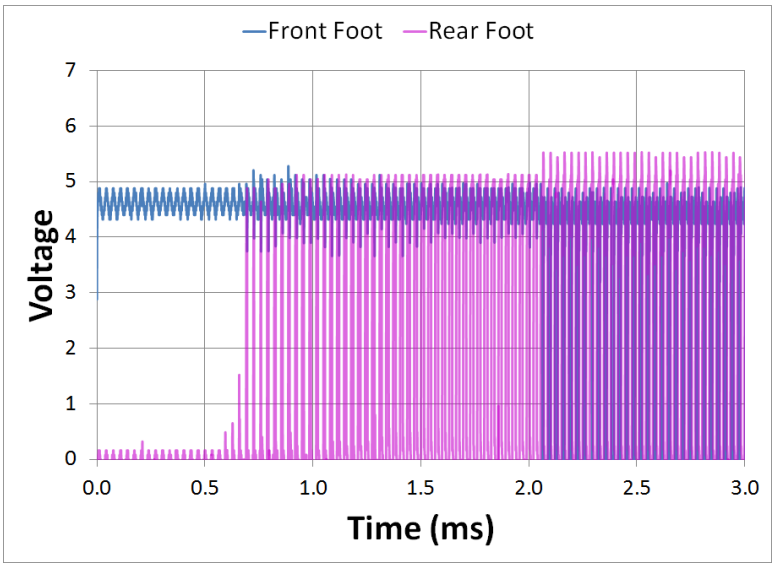

Figure 8. Transient state behavior of crawler taken with contact plates.

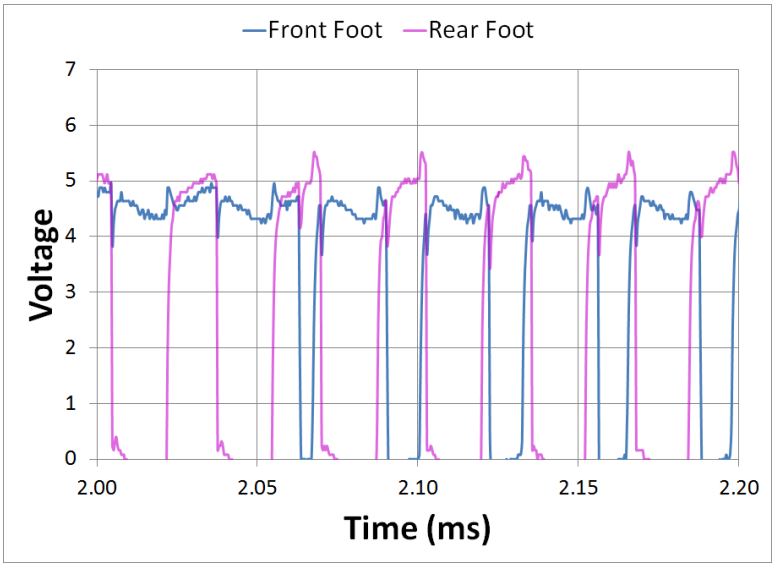

Figure 9. Steady state type behavior taken with contact plates.

The same contact plate is run for the crawler in the third mode. However, due to the amplitude being more then an order of magnitude smaller and the decrease in velocity, the crawler does not move across the copper plate. The roughness of the copper plate likely is another contributing factor to the lack of cadence data in the third mode.

Figure 7b shows another set-up involving two sets of parallel copper plates. The plates are used as inputs to a PIC microcontroller running a simple timer and LCD display. Used in conjunction with the copper plates, a time to traverse one set of copper patches to the other is obtained. This setup is used to first determine the kinetic friction coefficient of the three surfaces shown in Figure 3 using a tilt test [3] and an unpowered crawler. The platform is then levelled and the crawler powered to determine the steady-state velocity of the same crawler. The averaged velocities can be found in Table 4 with the rest of the contact data.

Similar to the contact plate data, velocity data is not easily measured due to the drastic decrease in speed from the forwards to the reverse modes. Only through placing the actuator on a very smooth graphite surface, can steady movement in the

Table 4. Experimentally obtained friction coefficients and averaged steady-state behaviors.

Comparison of Contact Duration			
Material	*Dynamic Coefficient of Friction*	*Duty Cycle Front/ Rear*	*Steady-State Velocity*
Delrin	0.25	32%/ 51%	0.048 m/s
Nylon	0.30	32%/ 51%	0.067 m/s
Plexiglas	0.50	32%/ 51%	0.110 m/s

backwards direction to be seen. Through visual inspection and the use of a stopwatch, the crawler is measured to move at an averaged 1 mm/s. This bodes well with the information found via finite element that predicts a steady state speed of 0.7 mm/s (Figure 6b).

11. CONCLUSION

It is uncommon in articles that a full transient, multiphysics, contact problem is accurately described. Coupling the piezoelectric excitation with the vibration of the bar and superimposing that onto a contacting interface leads to problems with element interfacing, shear locking, proper damping specifications, and transient convergence to name a few. It is no wonder then that many authors look at very discrete events within contact problems to obtain a quasi-static answer. This paper takes the unique approach of solving for all of these problems simultaneously in the analysis of the single-phase, piezoelectric, crawler actuator.

Through the use of ANSYS 14 APDL, forwards and backwards movement of this simple crawler has been proven operating in the first and third modes, respectively. Though simplified in build and geometry, the transient and steady-state solutions demonstrate the complex relationship between foot cadence and steady-state behavior. The results show that many of the driving variables exhibited in Figure 6 show anything but steady state behavior, the net behavior of the crawler

is one that tends toward stability. The combination of the crawler's additive and subtractive frictions reaching equilibrium, the crawler reaching a steady contact time for each foot, and the foot kinematics all play a contributing role to reaching steady-state. Contact duration and velocities are corroborated with experimental means, through the use of copper contact devices. Additionally, the bidirectional behavior of this crawler is proven, though magnitudes slower does open possibilities for future studies.

SECTION

2. CONSLUSIONS

The crawler SWUM has shown that an actuator of simple design can demonstrate complex behaviors. This paper takes the unique approach of analyzing the kinematics of a bouncing and vibrating body, which from the outcome of this study demonstrates that there are differences with similar studies of bouncing bodies. Papers involving preloads or rigid objects rebounding on bouncing platforms show instabilities at accelerations much higher then gravity. Most analyses of this type stay far below the acceleration of gravity region to avoid such stochastic behaviors.

The stability of this crawler is shown and is proven that given a wide array of damping parameters and initial heights, the crawler inevitably reaches a state of periodicity. What this means is if a surface can accurately be modeled as rigid with a coefficient of restitution, this crawler would have steady and predictable behavior. Some bouncing is expected initially with primary driving variables being the initial kinematic state, excitation amplitude, and foot cadence. Landing at the boundary of the absorb/transmit region means that little energy is transmitted through the stator-rotor with the net outcome being a decay of the bouncing. This is shown to be the case for the crawler contacting multiple surfaces. The next step in this study will be a full parametric examination of the stochastic behavior of this crawler. Variables like the length, foot placement, and excitation will be varied to evaluate the robustness of the stability claimed in this paper.

It is uncommon in articles that a full transient, multiphysics, contact problem is accurately described. Coupling the piezoelectric excitation with the vibration of the bar and superimposing that onto a contacting interface can lead to problems

with element interfacing, shear locking, proper damping specifications, and transient convergence to name a few. It is no wonder then that many authors look at very discrete events within contact problems to obtain a quasi-static answer. This paper takes the unique approach of solving for all of these problems simultaneously in the analysis of the single-phase, piezoelectric, crawler actuator. Through the use of ANSYS 14 APDL, forwards and backwards movement of this simple crawler has been proven operating in the first and third modes modes, respectively. Though simplified in build and geometry, the transient and steady-state solutions demonstrate the complex relationship between foot cadence and steady-state behavior. The results show that many of the driving variables exhibited show anything but steady state behavior, however the net behavior of the crawler is one that tends toward stability. The combination of the crawler's additive and subtractive frictions reaching equilibrium, the crawler reaching a steady contact time for each foot, and the foot kinematics all play a contributing role to reaching steady-state. Contact duration and velocities are corroborated with experimental means, through the use of copper contact devices. Additionally, the bidirectional behavior of this crawler is proven, though magnitudes slower does open possibilities for future studies.

BIBLIOGRAPHY

[1] J.R. Allik, H.; Hughes. Finite element for piezoelectric vibration. *International Journal Numerical Methods of Engineering*, NO.2:151–157, 1970.

[2] ANSYS, Inc. *ANSYS Mechanical APDL Theory Reference*, 14.0 edition, November 2011.

[3] ASTM International. *G1115-10 Standard Guide for Measuring and Reporting Friction Coefficients*, book of standards volume: 03.02 edition, 2012.

[4] Klaus-Jrgen Bathe. *Finite Element Procedures*. Englewood Cliffs, N.J.: Prentice Hall, 1996.

[5] S. Dorbolo, D. Volfson, L. Tsimring, and A. Kudrolli. Dynamics of a bouncing dimer. *Phys. Rev. Lett.*, 95:044101, Jul 2005.

[6] J.M. Fernandez and Y. Perriard. Comparative analysis and modeling of both standing and travelling wave ultrasonic linear motor. In *Ultrasonics, 2003 IEEE Symposium on*, volume 2, pages 1770 – 1773 Vol.2, oct. 2003.

[7] J.R. Friend, J. Satonobu, K. Nakamura, S. Ueha, and D.S. Stutts. A single-element tuning fork piezoelectric linear actuator. *IEEE Transactions on Ultrasonics, Ferroelectrics and Frequency Control*, 50(2):179 –186, feb. 2003.

[8] P. Hagedorn and J. Wallaschek. Travelling wave ultrasonic motors, part i: Working principle and mathematical modelling of the stator. *Journal of Sound and Vibration*, 155(1):31 – 46, 1992.

[9] Siyuan He, Weishan Chen, Xie Tao, and Zaili Chen. Standing wave bi-directional linearly moving ultrasonic motor. *IEEE Transactions on Ultrasonics, Ferroelectrics and Frequency Control*, 45(5):1133 –1139, sep 1998.

[10] Katsumi Kakizaki and Yutaka Ajiro. Remote controlled toy utilizing piezoelectric element, Sep. 16, 1986.

[11] A. Kawamura and N. Takeda. Linear ultrasonic piezoelectric actuator. *IEEE Transactions on Industry Applications*, 27(1):23 –26, jan/feb 1991.

[12] Tae-Yoal Kim, Beom-Jin Kim, Tae-Gone Park, Myong-Ho Kim, and Kenji Uchino. Design and driving characteristics of ultrasonic linear motor. *Ferroelectrics*, 263(1):113–118, 2001.

[13] Kyongjai Lee, Dong-Kyun Lee, S. Borodinas, P. Vasiljev, S. Nahm, and Seok-Jin Yoon. Analysis of shaking beam actuator for piezoelectric linear ultrasonic motor. *IEEE Transactions on Ultrasonics, Ferroelectrics and Frequency Control*, 51(11):1508 –1513, nov. 2004.

[14] Kuang-Chen Liu, James Friend, and Leslie Yeo. Rotating bouncing disks, tossing pizza dough, and the behavior of ultrasonic motors. *Phys. Rev. E*, 80:046201, Oct 2009.

[15] Wei; Song Chongmin Luo, Zhen; Gao. Design of multi-phase piezoelectric actuators. *Journal of Intelligent Material Systems and Structures*, 21:1851–1865, 2010.

[16] T. Maeno, T. Tsukimoto, and A. Miyake. Finite-element analysis of the rotor/stator contact in a ring-type ultrasonic motor. *IEEE Transactions on Ultrasonics, Ferroelectrics and Frequency Control*, 39(6):668 –674, nov 1992.

[17] P. Le Moal and P. Minotti. A 2-d analytical approach of the stator-rotor contact problem including rotor bending effects for high torque piezomotor design. *European Journal of Mechanics, A/Solids*, 16:1067–1103, 1997.

[18] T Sashida. Motor device utilizing ultrasonic oscillation, 1984-05-16.

[19] Werner Soedel. *Vibrations of Shells and Plates*. Marcel Dekker, 3 edition, 2004.

[20] P. Vasiljev, D. Mazeika, and G. Kulvietis. Modelling and analysis of omnidirectional piezoelectric actuator. *Journal of Sound and Vibration*, 308(3-5):867 – 878, 2007. Vibro-Impact Systems.

[21] H. S. Wright, Michael R. Swift, and P. J. King. Stochastic dynamics of a rod bouncing upon a vibrating surface. *Phys. Rev. E*, 74:061309, Dec 2006.

[22] Chungsheng Zhao. *Ultrasonic Motors: Technologies and Applications*. Science Press, Beijing, 2011.

[23] Bernard Brogliato Zhen Zhao, Caishan Liu. Planar dynamics of a rigid body system with frictional impacts. ii. qualitative analysis and numerical simulations. *Proceedings of The Royal Society*, 465(2107), 2009.

[24] Yong Zhou, Beiyue Zhou, and Shi Li. Driving performance analysis of a novel piezoelectric actuator. In *Measuring Technology and Mechatronics Automation (ICMTMA), 2010 International Conference on*, volume 2, pages 34 –37, march 2010.

VITA

Dwight Santiago Maness was born on August of 1987 in Olongapo, Philippines. As a child of a navy serviceman, he lived in various Pacific islands before settling in Missouri to attend college. He began his college career in Fall 2005 at East Central College in Union, where he stood as student council representative to the pre-engineering club for two years. In May 2007 he transferred to what is now the Missouri University of Science and Technology (MS&T formerly University of Missouri-Rolla) to finish his bachelors degree in Mechanical Engineering. While at MS&T he joined the Missouri Satellite Team, becoming a member of the structures subsystem for two years and the lead of the communications subsystem for his final year. In Fall 2010 he graduated with his B.S. in Mechanical Engineering with magna cum laude honors. Soon after he began work under Dr. Daniel S. Stutts to earn his Masters degree studying piezoelectrics, vibrations, and embedded systems. Dwight also taught a controls lab course for two years, involving the use of instrumentation and Programmable Logic Controllers (PLC). In May 2013 he recieved his Masters degree and currently works at Intelligrated as an Electrical Engineer.